PHYSICAL REVIEW B VOLUME 50, NUMBER 19 15 NOVEMBER 1994-I

Electronic transport in metallic iron disilicide

K. Kyllesbech Larsen, M. Van Hove, A. Lauwers, R. A. Donaton, K. Maex, and M. Van Rossum
Interuniversity Micro-Electronics Center (IMEC), Kapeldreef 75, B-3001 Leuven, Belgium
(Received 31 May 1994)

Measurements of the electrical resistivity, Hall effect, and magnetoresistance are reported for metallic iron disilicide layers, fabricated by ion-beam synthesis (IBS) and solid-state reaction (SSR) on (100)Si. The analysis of the data is consistent with three-dimensional weak-localization theories, including a strong spin-orbit interaction, and electron-electron interaction. The spin-orbit scattering and electron wave-function dephasing rates are extracted from nonlinear least-squares fits to the magnetoresistance and the low-temperature electrical resistivity. From both the magnetic field and temperature dependence it is found that the electron-electron interaction due to spin-splitting effects also contributes to the scattering in this material. For IBS and SSR fabricated iron disilicide layers the dephasing rate saturates below 4.2 K indicating a scattering contribution from magnetic impurities, and varies as T^p above 4.2 K. From the magnetoresistance measurements in the temperature range between 20 and 50 K, the exponent of the dephasing rate is found to be about 3 in agreement with electron-phonon interband scattering being dominant, consistent with the overall temperature dependence of the resistivity at zero magnetic field.

I. INTRODUCTION

The transition-metal silicides are very important in microelectronics, where they are used as gate metallization in very-large and ultralarge scale integration technologies, and recently work on silicide solar cells and infrared detectors has progressed. The major scientific effort has been concentrated on the characterization of the silicide/silicon interface properties and the silicide formation mechanisms, such as the kinetics of growth, epitaxy, and thermal stability. Thus, the structural, thermodynamic, and kinetic aspects of silicides are in many respects well understood.[1–3] However, not as much work has been done to characterize the fundamental electronic properties with respect to the scattering mechanisms in the transition-metal silicides.[4,5] The basic scattering mechanisms in silicides and the contribution to the transport properties, such as the electrical resistivity, magnetoresistance, Hall effect, and thermopower, are far from well understood. The free-electron based models can no longer fully describe the transport properties because of the transition-metal component. Contributions to the scattering might come from d-band conduction, s-d hybridization, skew scattering, and side jump.[6] Furthermore, for high resistivity and strongly disordered silicides strong elastic scattering occurs, and quantum corrections to the electrical resistivity have to be considered. Such corrections can arise from weak localization[7] (WL), spin-orbit interaction[8] (SOI), electron-electron interactions[9] (EEI), and superconducting fluctuations[10] (SCF). These effects are not considered in the Boltzmann-transport equation, which is commonly used to describe the electronic transport in silicides. The quantum correction theories allow a quantitative determination of, for example, the dephasing and spin-orbit scattering rates. Although the quantum corrections to the electrical transport should be most strongly manifested in low-dimensional systems[11] because of the reduction of the phase-space dimension, they have recently been observed in bulk amorphous materials[12,13] and icosahedral alloys.[14,15] Furthermore, a recent study of amorphous vanadium silicon[16] with silicon contents above 50 at. % showed evidence of weak-localization effects influenced by a strong SOI.

The metallic iron disilicide has a tetragonal crystal structure belonging to the space group $P4/MMM$ with lattice constants $a=b=0.2690$ nm and $c=0.5134$ nm. In this paper we present a study of the electrical properties, such as the resistivity, Hall effect, and magnetoresistance of metallic polycrystalline iron disilicide (α-$FeSi_2$) layers fabricated both by ion-beam synthesis[17] (IBS) and solid-state reaction (SSR) of iron-titanium-silicon diffusion couples.[18] The results show that WL, SOI scattering, and EEI due to scattering from the particle-hole channel have to be taken into account in order to explain the low-temperature behavior of the electrical resistivity and magnetoresistance data.

II. THEORETICAL BACKGROUND

For low-resistivity transition-metal silicides having a residual resistivity less than 100 $\mu\Omega$ cm the electrical transport properties can normally be described by the Boltzmann-transport equation, where the scattering due to s or d electrons can be treated as perturbations. In most cases the electrical resistivity of a transition-metal silicide is analyzed based on Matthiesen's expression[5] $\rho(T)=\rho_0+\rho_{e-\mathrm{ph}}(T)$, where ρ_0 is the residual resistivity, and $\rho_{e-\mathrm{ph}}(T)$ is the electron-phonon contribution to the electrical resistivity given by the Bloch-Grüneisen theory:[19]

 ©1994 The American Physical Society

$$\rho_{e-\text{ph}}(T)=\rho'\Theta\left[\frac{T}{\Theta}\right]^n \times\int_0^{\Theta/T}\frac{z^n}{[\exp(z)-1][1-\exp(-z)]}dz =\rho'\Theta\left[\frac{T}{\Theta}\right]^n G_n\left[\frac{\Theta}{T}\right], \quad (1)$$

where ρ' is a prefactor that includes the electron-phonon coupling strength, and Θ is the effective Debye temperature. The exponent n is dependent on the dominant scattering mechanisms, and takes the value 5 for electron-phonon intraband scattering and 3 for electron-phonon s-d interband scattering.

In materials with high electrical resistivities the elastic mean-free path is of the order of an interatomic distance. In this case the electrons do not travel in the classical trajectories as described by the Boltzmann-transport equation, and quantum corrections, resulting from interaction and interference effects between scattered electron waves, i.e., weak localization, must be taken into account. Assuming that the contributions from the quantum corrections to the electrical resistivity can be added, a modified Matthiesen expression $\rho(T)=\rho_0+\rho_{e\text{-ph}}(T)+\rho_{\text{QCR}}(T)$ is obtained, where $\rho_{\text{QCR}}(T)$ is the term describing the quantum corrections to the resistivity. It should be emphasized that the interference and interaction effects described below are all represented by the first term in a perturbation expansion in the disorder parameter $(k_F L_0)^{-1}$ (i.e., k_F is the Fermi wave vector and L_0 is the elastic mean-free path). Thus the quantum corrections described here are in principle only applicable for weakly disordered systems when $k_F L_0 \gg 1$. However, it has recently been shown that higher-order terms only become significant when $k_F L_0$ becomes very close to one.[20] In addition, complications might also arise from the fact that two types of carriers, namely, s and d electrons, exist in transition-metal based alloys, where d-electron states can account for more than 80% of the conductivity.[21] It has been shown that the interference theories can apply to systems with multiple carriers. In this case an average Fermi surface and a weighted density of the different carriers have to be used[22] in analyzing the electrical transport.

First, a discussion on the influence of a magnetic field on the electrical resistivity and the corresponding quantum corrections to the resistivity will be given. Second, the corresponding temperature-dependent quantum corrections in the absence of a magnetic field will be treated.

A. Weak localization and spin-orbit interaction

1. Magnetic field dependence

The expression for the magnetoresistance of a noninteracting electron gas due to weak localization in the presence of spin-orbit interaction is given by[8,23]

$$\left[\frac{\Delta\rho}{\rho^2}\right]_{\text{WL}}=\frac{\rho(T,H)-\rho(T,H=0)}{\rho^2(T,H=0)} =\frac{\sigma_{00}}{2}\left[\frac{eH}{\hbar}\right]^{1/2}\left[1+2\beta(T,H)F_3\left[\frac{H}{H_\phi}\right] -3F_3\left[\frac{H}{H_\phi+2H_{\text{SO}}}\right]\right], \quad (2)$$

with T being the temperature, H the magnetic field, and $\sigma_{00}=e^2/2\pi^2\hbar$ the universal conductance (i.e., $\sigma_{00}\approx\frac{1}{81}$ kΩ^{-1}). The field strengths H_ϕ and H_{SO} are defined as

$$H_x=\frac{\hbar}{4eD}\tau_x^{-1} \quad (x=\phi,\text{SO}), \quad (3)$$

where τ_ϕ and τ_{SO} are the electronic relaxation times for the dephasing and spin-orbit interaction, respectively. Furthermore, D is the electronic diffusion constant, and $\beta(T,H)$ is the Maki-Thompson function describing superconducting fluctuations due to interactions of electrons with fluctuating Cooper pairs.[24,25] The Maki-Thompson conductivity can contribute to the magnetoresistance even at temperatures above the superconducting transition temperature, but disappears if, for example, magnetic impurities are present in the material. The F_3 function is a function which describes the interaction between electronic wave functions in a three-dimensional system.[26] An approximate analytical expression for F_3 has been given by Ousset *et al.*[27] Complex behavior of the magnetoresistance is observed and predicted if both the dephasing scattering contribution and the spin-orbit interaction are present. Several characteristic length scales are relevant in order to estimate the importance of the different scattering contributions to the magnetoresistance. The elastic mean-free path is defined in the free-electron limit as $L_0=\hbar k_F/ne^2\rho$, where n is the carrier concentration. The coherence length,[28] defined as $L_\phi=\sqrt{D\tau_\phi}$, is the diffusion length of the electron before it encounters a dephasing inelastic collision. The inelastic scattering introduces stochastic fluctuations in the time evolution of the electronic wave function. These fluctuations, as argued by Thouless,[28] will limit the quantum interference necessary for localization, and the localization effects are cut off beyond the coherence length. Thus to observe interference effects L_ϕ has to exceed the elastic mean-free path L_0. A magnetic field will have the effect of inducing destructive interference between the electronic partial wave functions, and suppresses the localization effect. The relevant length scale to compare with is the Landau orbit size $L_H=\sqrt{\hbar/2eH}$. Destructive interference can be expected when the coherence length and the Landau orbit size become comparable, and a negative magnetoresistance will result. If the spin-orbit interaction, with a spin-orbit mean-free path defined as $L_{\text{SO}}=\sqrt{D\tau_{\text{SO}}}$, also contributes to the quantum corrections, an additional complexity is encountered in magnetoresistance. Depending on the relative size of L_H, L_ϕ, and L_{SO}, both positive ($L_\phi \gg L_{\text{SO}}$) and negative

($L_\phi \le L_{SO}$) magnetoresistances are possible, and the behavior can be experimentally investigated by, for example, the magnetic field and temperature dependence of the electrical resistivity.[29]

2. Temperature dependence

Fukuyama and Hoshino[8] have derived the temperature-dependent localization correction to the electrical resistivity given by the particle-particle diffusion process[30]

$$\left[\frac{\Delta\rho}{\rho^2}\right]_{WL} = \frac{\rho(T)-\rho(T=1.2\text{ K})}{\rho^2(T=1.2\text{ K})} = -\sigma_{00}\left[\frac{e}{\hbar}\right]^{1/2}\left[3\sqrt{\tfrac{4}{3}H_{SO}+H_\phi(T)} - \sqrt{H_\phi(T)}\right] . \quad (4)$$

The temperature dependence of the dephasing field strength is given by the relation

$$H_\phi(T) = \frac{\hbar}{4eD} A_\phi T^{p_\phi} , \quad (5)$$

where A_ϕ and p_ϕ are the dephasing scattering rate amplitude and exponent, respectively. The value of the exponent p_ϕ, obtained by nonlinear least-squares fitting to Eq. (4), is an indicator for the dominant scattering mechanism. From Eq. (4) it can be seen that the presence of a strong spin-orbit interaction will tend to delocalize the electrons and reduce the electrical resistivity. Several different power-law behaviors have been predicted and observed depending on the underlying scattering mechanisms. If, for example, the electron-phonon interband scattering is dominant, an exponent of 3 should be observed. However, if electron-electron interaction is dominating due to scattering from particle-particle or particle-hole channels, an exponent of 1.5 is expected. If several different scattering mechanisms are contributing simultaneously to the scattering rate, the effective exponent is in the range between 1.5 and 3. A major complication in obtaining reliable exponents occurs when magnetic impurities are present in the material, because these could hide the real power-law behavior at the lowest temperatures. The temperature dependence of the dephasing rate can also be obtained from the dephasing relaxation time obtained from magnetoresistance measurements.

B. Electron-electron interactions

1. Magnetic field dependence

In contrast to the localization effects described above which involve single electrons, the Coulomb contribution arises from electron-electron interaction in the presence of multiple-scattering processes in a given material. Two contributions to the electrical resistivity have been treated. One originates from the particle-particle channel describing electron-orbital effects,[31] and the other from the particle-hole channel[9] describing the spin splitting of the conduction-electron energies. It can be shown that the electron orbital part does not contribute significantly to the resistivity at temperatures above 4.2 K, and, because of that, this scattering process will not be discussed in this paper. The contribution to the magnetoresistance from electron-electron interactions assuming scattering in the particle-hole channel is given by

$$\left[\frac{\Delta\rho}{\rho^2}\right]_{EEI} = \frac{\sigma_{00}}{2}\tilde{F}\left[\frac{k_B T}{2\hbar D}\right]^{1/2} g_3\left[\frac{g\mu_B H}{k_B T}\right] . \quad (6)$$

In this expression $\tilde{F}$ is the effective Coulomb screening factor that can take the value 0 for no screening and 1 for complete screening, g is the Landé factor, μ_B is the Bohr magneton, and k_B is the Boltzmann constant. It should be mentioned that the theoretical derivations of the electron-electron contributions are based on the assumption that $\tilde{F} \ll 1$. The function g_3 is describing the electron-electron interaction in the diffusion channel, and an analytic approximation has been given by Ousset *et al.*[27] It has been shown that the electron-electron interaction, such as the electron-orbital motion and the Zeeman spin-splitting effects, can be reduced by as much as 25% due to strong spin-orbit interaction in a two-dimensional system.[32] The effect of the spin-orbit interaction on the electron-electron interaction in a three-dimensional system has been investigated by Sahnoune, Ström-Olsen, and Fischer[33] where it was shown that the EEI contribution to the magnetoresistance is greatly reduced and can even disappear at large spin-orbit scattering rates.

2. Temperature dependence

The temperature dependence due to scattering from the particle-hole channel[29] is given by the expression

$$\left[\frac{\Delta\rho}{\rho^2}\right]_{EEI} = -0.915\frac{\sigma_{00}}{2}\left[\frac{4}{3}-\frac{3}{2}\tilde{F}\right]\left[\frac{k_B T}{\hbar D}\right]^{1/2} . \quad (7)$$

Even if $\tilde{F}$ is very small EEI's can contribute significantly to the electrical resistivity providing the diffusivity is comparably small, and will cause a decrease in the resistivity with increasing temperature. Thus the temperature dependence of the resistivity might be a better probe for the EEI's than the magnetoresistance where either very low temperatures or high magnetic fields are required.

III. EXPERIMENT

The ion-beam synthesis of the iron disilicide was performed on ⟨100⟩ *n*-type silicon 5-in.-diam wafers. Implantations of 200-keV Fe^+ were performed in a vacuum better than 7×10^{-8} Torr, with a dose of 3×10^{17} Fe^+/cm^2 at 500 °C. The temperature during the implantation was regulated by a resistively heated chuck. The implant temperature was monitored *in situ* and in real time by an optical-fiber sensor.[34] After the implantation the samples were annealed at 1150 °C for 30 s in a highly purified N_2 ambient resulting in a polycrystalline α-$FeSi_2$ buried layer. For the solid-state reacted α-$FeSi_2$ an Fe-Ti

bilayer on top of a ⟨100⟩ oriented silicon wafer was sputtered by sequential deposition using a Balzer BAS-450 dc-magnetron system. The use of this bilayer has the advantage of making a cleaner reaction between the iron and the silicon substrate, where the role of the intermediate titanium layer is to act as a diffusion barrier[35] for silicon and iron, lowering the reaction rate, and to act as getter for oxygen contamination on the silicon surface. It has been shown using the bilayer silicidation technique that the resulting silicide layer is structurally superior compared to iron disilicide layers fabricated without the intermediate Ti layer.[36] The presputtering pressure was typically better than 4×10^{-6} Torr. After the sputtering the silicidation was carried out by rapid thermal annealing at 1050 °C for 30 s. The unreacted (i.e., with respect to the silicon substrate) metal layer was selectively etched off.

Rutherford backscattering spectrometry (RBS) was used to check the homogeneity of the films and to determine their composition and thicknesses. The composition of the films could be determined within 1 at. %. The error on the absolute values of the electrical resistivities reported in this paper, arising mainly from the uncertainty in the thickness determination, is estimated to be less than 10%. The composition of the iron disilicide was for all layers found to yield an iron deficiency of 6 at. % giving a stoichiometry of $Fe_{0.75}Si_2$. The reason for this deficiency is that the α-$FeSi_2$ phase can accommodate a considerable number of Fe vacancies, being a phase with a finite phase field.[37] The thicknesses are 100 nm for the IBS fabricated layer, 70 and 35 nm for the SSR layers. From the Auger electron spectroscopy (AES) analysis of the solid-state reacted layers, done after the etching procedure, no titanium was found on top of the layers. Furthermore, AES sputter depth profiling showed no traces of titanium and oxygen in the solid-state reacted α-$FeSi_2$ layer within the resolution of AES which is about 1 at. %. In addition, secondary ion-mass spectrometry depth profiling was used, because of its superior sensitivity compared to AES and RBS, and showed a Ti content of less than 0.1 at. % to be present in the solid-state reacted iron disilicide layers. X-ray diffraction (XRD) was used to structurally characterize the thin iron disilicide layers. For all layers only the metallic α-$FeSi_2$ phase was found to be present. Several orientations were identified by XRD showing that the specimens are polycrystalline.

The electrical characterization was carried out in an Oxford SM4-7 ^{4}He-cryostat system that covers the temperature range from 1.2 to 300 K, and magnetic fields up to 7 T. The magnetic field is provided by a superconducting NbTi solenoid. A Hall bar geometry was defined by optical lithography and wet etching for the buried layer. The SSR layers where made on oxide patterned wafers with a 350-nm-thick thermal grown oxide. Hall bars were defined in the thermal oxide by optical lithography. Different materials have been used to ensure Ohmic contacts to the silicide layers. No influence of the contact material on the transport properties of the iron disilicide was found. Both for the IBS and the SSR layers reported in this paper, aluminum was used as the contact material. The electrical resistivity, Hall effect, and magnetoresistance were measured on Hall bars by the classical four-point probe techniques. The magnetoresistance was measured three times at each temperature in order to check for the reproducibility. The error on the absolute resistance was found to be less than 10% at fields lower than 1 T and less than 5% at higher fields. During the magnetic field scans the temperature was kept stable to within 1%. To avoid nonlinear effects at the lowest temperatures, such as heating up of the sample, currents between 10 μA and 1 mA were applied. However, no difference in the measured data except for a lower signal-to-noise ratio was observed using lower currents. The resistance and Hall effect measurements were performed with a current of 100 μA in order to have a good signal-to-noise ratio.

IV. ANALYSIS AND RESULTS

In Figs. 1 and 2, the electrical resistivity of α-$FeSi_2$ fabricated by both IBS and SSR is shown as a function of temperature. For the thinnest α-$FeSi_2$ (35 nm) fabricated by SSR the resistivity is much higher than for the thicker layers fabricated by SSR (70 nm) and IBS (100 nm). The thinnest layer (35 nm) has the highest residual resistivity of 511 $\mu\Omega$ cm compared to 277 $\mu\Omega$ cm for a 70-nm-thick iron disilicide layer, and 228 $\mu\Omega$ cm for 100-nm layer. The resistivity ratio $\rho_{300\,K}/\rho_{1.2\,K}$ is found to be ≈ 1.08

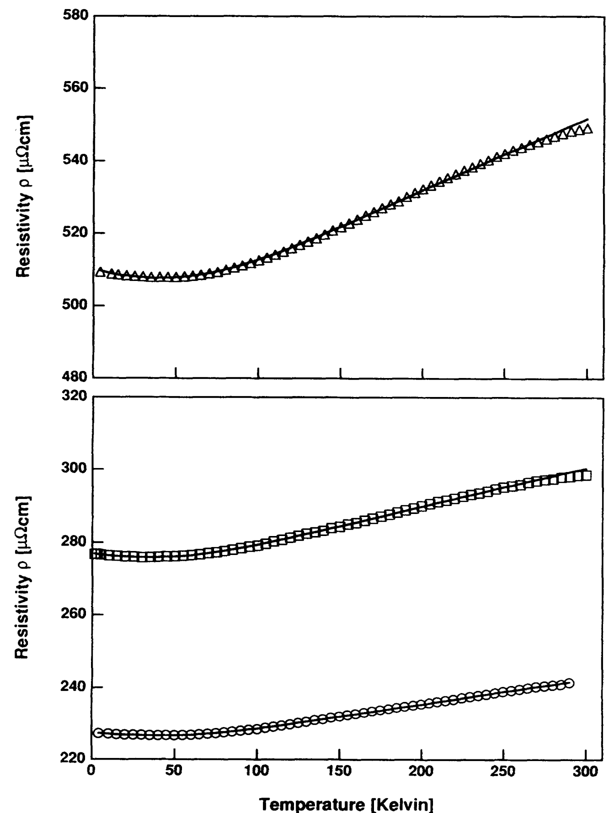

FIG. 1. Temperature dependence of the electrical resistivity of polycrystalline α-$FeSi_2$ fabricated by ion-beam synthesis (○, 100 nm thick), and solid-state reacted (□, 70 nm and △, 35 nm).

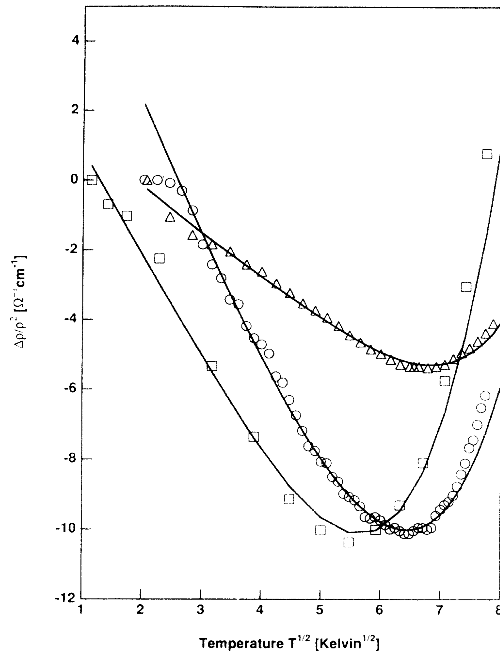

FIG. 2. The low-temperature dependence of the electrical resistivity showing a decrease in the resistivity vs the square root of the temperature. The symbols denote (○, 100 nm thick) IBS α-$FeSi_2$, and (□, 70 nm and △, 35 nm) SSR α-$FeSi_2$.

for all the samples. In Fig. 2 the details of the low-temperature behavior of the electrical resistivity are shown for the three different samples. In all silicide layers a minimum in the resistivity is found at about 40 K, and an increase in the resistivity following approximately a $\sqrt{T}$ dependence below the minimum is observed. For the thickest α-$FeSi_2$ layers (i.e., 100 and 70 nm) the increase in resistivity at the lowest temperatures is approximately the same although a small difference in the minimum temperature is observed. For the thinnest α-$FeSi_2$ layer (i.e., 35 nm) the increase is smaller and the minimum is also slightly shifted from the other samples. This low-temperature behavior of the electrical resistivity cannot be described by the Boltzmann-transport equation, where it is expected that the resistivity decreases with decreasing temperature and saturates at the residual resistivity. However, such a temperature behavior is expected when quantum effects influence the transport properties. The solid lines in Figs. 1 and 2 are nonlinear least-squares fits to Matthiesen's expression $\rho(T)=\rho_0+\rho_{QCR}(T)+\rho_{e\text{-}ph}(T)$, where ρ_0 is the residual resistivity, $\rho_{QCR}(T)$ the quantum correction to the electrical resistivity given by the Bloch-Grüneisen theory [Eq. (1)]. Down to the temperature of the minimum resistivity the temperature behavior of the electrical resistivity is well described by the Boltzmann equation with electron-phonon interband scattering in good agreement with previous work.[38] Below the resistivity minimum the $\rho_{QCR}(T)$ term is included in the fitting of the low-temperature resistivity data. Both the dephasing and spin-orbit scattering rate have been obtained and are summarized in Table I, together with the scattering rates obtained from the magnetoresistance measurements. The solid-state reacted layers show a saturation in the electrical resistivity at the highest temperature. When the conduction-electron mean-free path becomes comparable with the interatomic spacing, and the electron-phonon interaction is the dominant scattering mechanism, the electrical resistivity will no longer increase linearly with the temperature. Instead, the electrical resistivity will saturate at the higher temperatures.[39,40] At room temperature the conduction-electron mean-free paths for the SSR layers are about 0.589 and 0.357 nm for the 70- and 35-nm layers, respectively, and are close to the lattice spacing of the α-$FeSi_2$. It is therefore not surprising that a saturation in the electrical resistivity is observed at the highest temperatures.

Figure 3 shows the magnetoresistance of a 100-nm ion-beam synthesized α-$FeSi_2$ [Fig. 3(a)], and a solid-state reacted α-$FeSi_2$ 70-nm-thick layer [Fig. 3(b)] as a function of the temperature. It should be emphasized that the observed magnitude of the magnetoresistance shown in Figs. 3(a) and 3(b) cannot be explained by the classical magnetoresistance which can be estimated to be at least four orders of magnitude lower than the observed magnetoresistance.[19] In both cases the magnetoresistance is

TABLE I. Physical parameters of the metallic $FeSi_2$ obtained by magnetoresistance and temperature dependence of the electrical resistivity.

Sample	$\rho_{1.2\,K}$ ($\mu\Omega$ cm)	$\rho_{300\,K}/\rho_{1.2\,K}$	$1/\tau_{SO}$ (10^{12} s^{-1})[a]	$1/\tau_{SO}$ (10^{12} s^{-1})[b]	$1/\tau_{\phi}$ (s^{-1})[a]	$1/\tau_{\phi}$ (s^{-1})[b]	$1/\tau_{\phi}$ (s^{-1})[c]
IBS $d=100$ nm	228	1.07	1.9	1.8	6–40 K: $6.6\times10^{7}T^{2.6\pm0.2}$	$7.6\times10^{6}T^{3.1\pm0.3}$	$2.3\times10^{6}T^{3}$
SSR $d=70$ nm	277	1.08	1.7	1.4	4.2–20 K: $1.2\times10^{10}T^{1.2\pm0.3}$ 20–50 K: $5.6\times10^{6}T^{3.3\pm0.3}$	$3.1\times10^{6}T^{2.4\pm0.4}$	$3.2\times10^{6}T^{3}$
SSR $d=35$ nm	511	1.08	0.9	0.7	$1.3\times10^{10}T^{1.1\pm0.1}$	$5.0\times10^{7}T^{2.5\pm0.4}$	$6.3\times10^{6}T^{3}$

[a]From the magnetoresistance.
[b]From the low-temperature dependence of the resistivity.
[c]Extracted from the Bloch-Grüneisen model.

positive and the magnitude decreases as a function of temperature. The field dependence of the magnetoresistance is at low fields approximately a square field dependence while a square root dependence is found at higher fields. This magnetic field dependence cannot be explained by the free-electron theory. Furthermore, considering the nonclassical behavior observed for the low-temperature electrical resistivity, which strongly indicates quantum effects due to strong elastic scattering effects, such a behavior can only be attributed to weak localization in the presence of a strong spin-orbit interaction as described by Eq. (2). The effect of the Coulomb interactions on the magnetoresistance is expected to be more significant in the high H/T limit, and with the relative low fields and high temperatures (i.e., $T > 1$ K) available in this experiment, difficult to detect. The magnitude of the magnetoresistance is lowered as the temperature is increased due to the enhanced inelastic scattering. The solid lines are nonlinear least-squares fits to Eqs. (2) and (6) showing an overall good agreement between the measurements and the localization and interaction models. It was found that the contribution from the Maki-Thompson function $\beta(T,H)$ is negligible and this parameter has been assumed to be zero in the evaluation. The superconducting fluctuations, described by the Maki-Thompson resistivity, are known to be destroyed by magnetic impurities. The magnetoresistance is found to be essentially independent of temperature at the lowest temperatures, indicating a constant dephasing-scattering rate. This implies that magnetic impurities giving rise to residual spin scattering are present in our silicide layers, but not in an amount to destroy the phase coherence of the partial electronic wave functions, and, furthermore, explains why the Maki-Thompson contribution is lacking. Thus there are only three fitting parameters, H_ϕ, H_{SO}, and $\tilde{F}$, if the electronic diffusivity is known. To extract the dephasing and spin-orbit relaxation times the electronic diffusivity has to be estimated, for example, by using the Einstein relation $D = 1/\rho e^2 N(E_F)$, where the density of states $N(E_F)$, evaluated at the Fermi energy E_F, can be deduced from Hall effect or low-temperature specific-heat measurements. In this work Hall measurements, as shown in Fig. 4, were carried out to extract the dominant carrier type, the effective carrier concentration, and the elastic mean-free path. This information is used in the assessment of the diffusivity. A positive Hall coefficient R_H was obtained for both IBS and SSR layers, indicating that holes are the dominant carrier type. Furthermore, R_H shows a slight temperature dependence in both layers as it decreases with increasing temperature, although the decrease is less for the SSR than the IBS layer. However, the Hall coefficient below 50 K is, within the uncertainty of the measurement, independent of temperature for both types of layers, indicating that essentially only one type of carrier is dominating the transport. The results of the Hall measurements are summarized in Table II. Because the effective mass of the hole carriers in α-$FeSi_2$ is not known, the electron rest mass has been assumed, and in what follows the

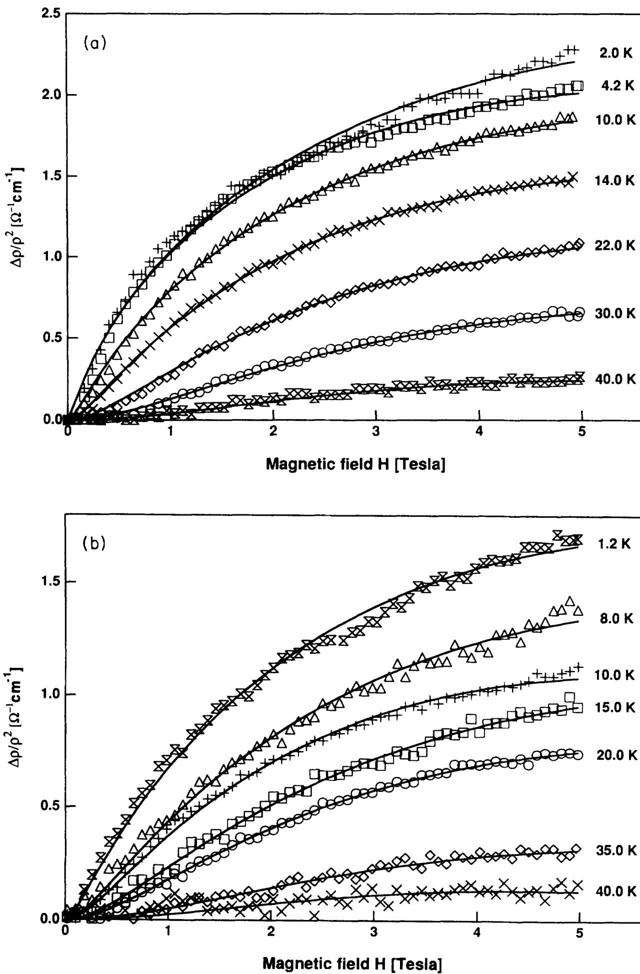

FIG. 3. The magnetoresistance data of polycrystalline α-$FeSi_2$. The points are the experimental data and the solid line a fit to the theory described in the text. Temperatures are indicated in the figures. (a) 100-nm IBS α-$FeSi_2$, (b) 70-nm SSR α-$FeSi_2$.

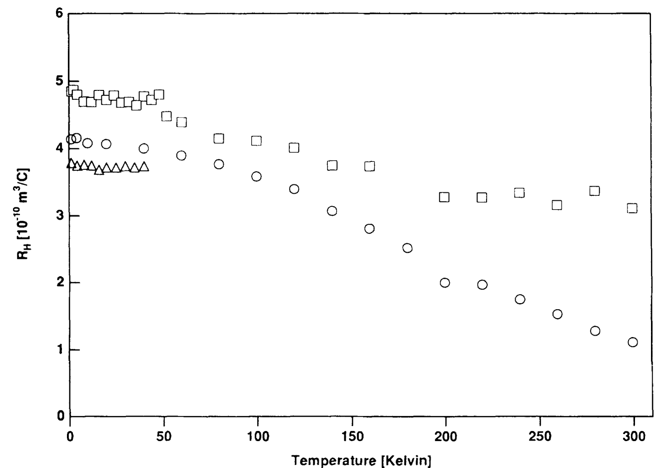

FIG. 4. The temperature dependence of the Hall coefficient R_H for IBS (○, 100 nm thick), and SSR (□, 70 nm and △, 35 nm) α-$FeSi_2$.

TABLE II. Experimental values derived from the Hall measurements assuming the nearly free-electron model. The electron diffusion constant D has been calculated according to the Einstein relation using the free-electron rest mass. The other parameters shown in the table are as follows: p the effective carrier concentration, L_0 the elastic mean-free path, k_F the Fermi wave vector, E_F the Fermi energy, and $N(E_F)$ the density of states.

Sample	p (10^{28} p/m^3)	L_0 (nm)	$k_F L_0$	E_F (eV)	$N(E_F)$ (eV^{-1} atom^{-1})	D (10^{-4} m^2 s^{-1})
IBS $d=100$ nm	1.51	0.90	7	2.23	0.40	2.70
SSR $d=70$ nm	1.29	0.83	9	2.00	0.38	2.31
SSR $d=35$ nm	1.66	0.38	3	2.38	0.42	1.17

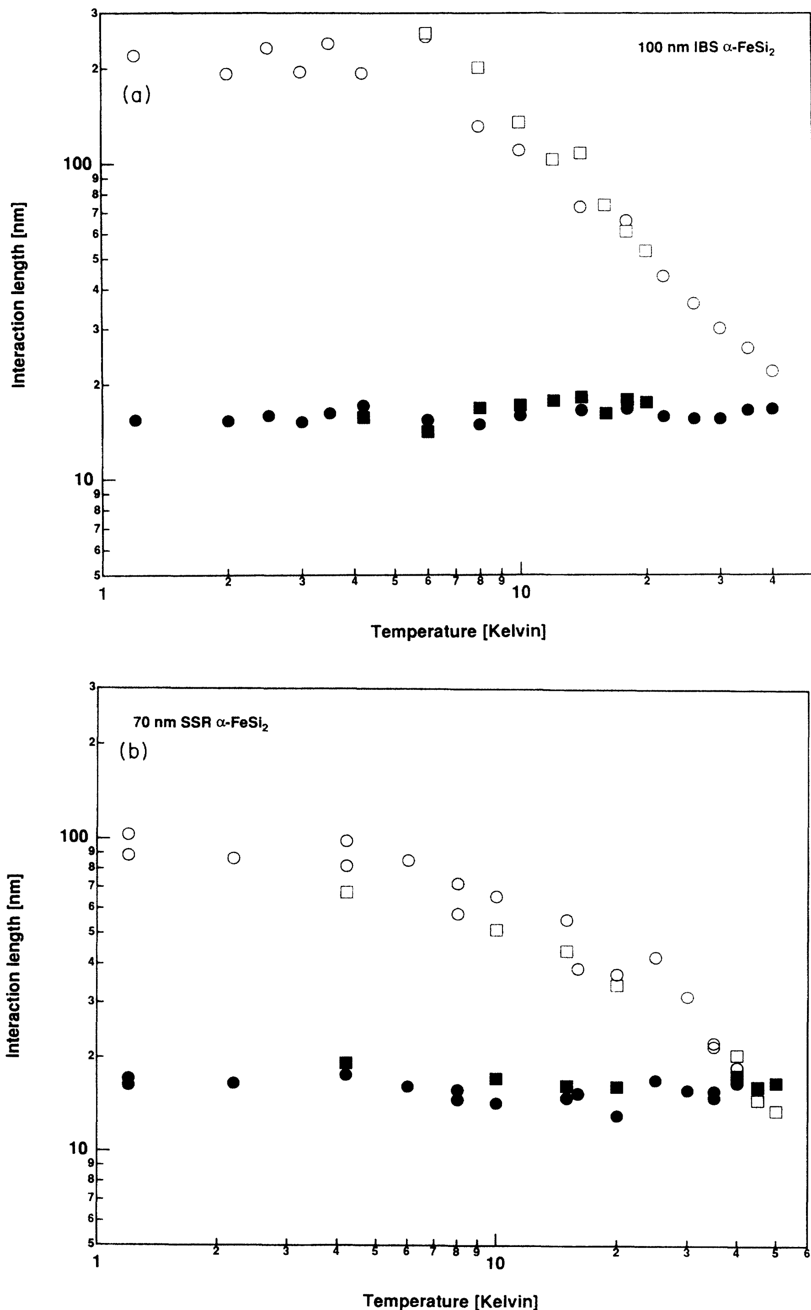

FIG. 5. The coherence length (open symbols) and spin-orbit mean-free path (closed symbols) shown as a function of temperature. (a) 100-nm IBS α-$FeSi_2$, (b) 70-nm SSR α-$FeSi_2$, and (c) 35-nm SSR α-$FeSi_2$.

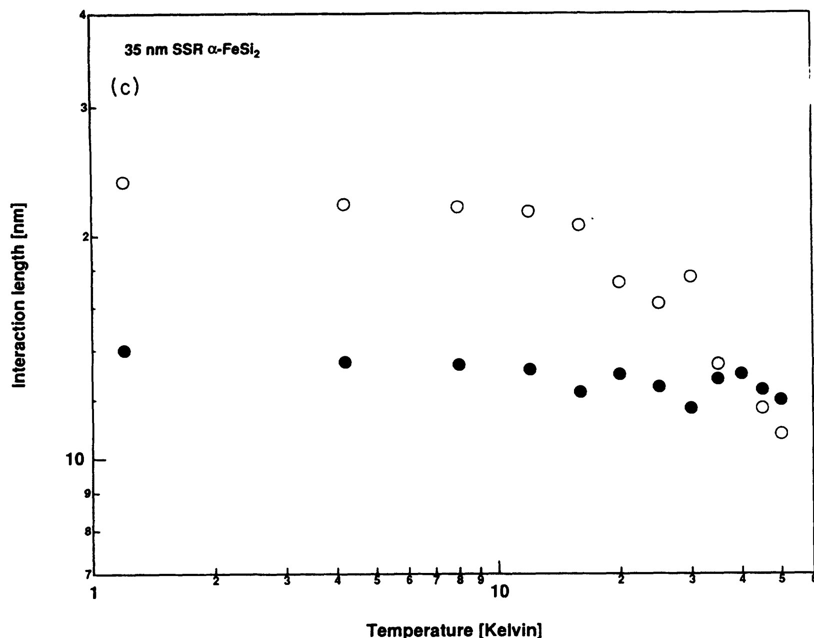

FIG. 5. (*Continued*).

diffusivity has been calculated using the experimentally derived density of state. It should be pointed out that this assumption may be in error, as recent band-structure calculations[41] of α-$FeSi_2$ indicate a higher effective hole mass. The experimental density of states $N(E_F)$ is found to be 0.40 ± 0.02 $eV^{-1}atom^{-1}$ for all the silicide layers. This result can be compared with the density of states estimated using the Friedel model[42] where $N(E_F)\approx2.07$ $eV^{-1}atom^{-1}$, or with a recent band-structure calculation where $N(E_F)\approx1.4$ $eV^{-1}atom^{-1}$. The discrepancy between the experimentally assessed and the theoretically derived value might be due to failure of the free-electron model, or to the fact that the effective hole mass m^* is larger than the rest mass m_0. Estimates of the density of states based on either the Friedel model or the band-structure calculation yield an m^*/m_0 ratio between 3 and 5, which is not unrealistically high. It should be pointed out that the assumption made about the hole mass only affects the density of states and makes the diffusivity higher than is the case using a higher effective hole mass. However, the assumption does not alter the conclusions made in this paper about the transport properties of the iron disilicide.

The results of the fitting to the magnetoresistance are summarized in Table I and in Fig. 5, showing the extracted coherence length (L_ϕ) and spin-orbit interaction mean-free path (L_{SO}) for IBS [Fig. 5(a)] and SSR [Figs. 5(b) and 5(c)] layers, respectively. The coherence length

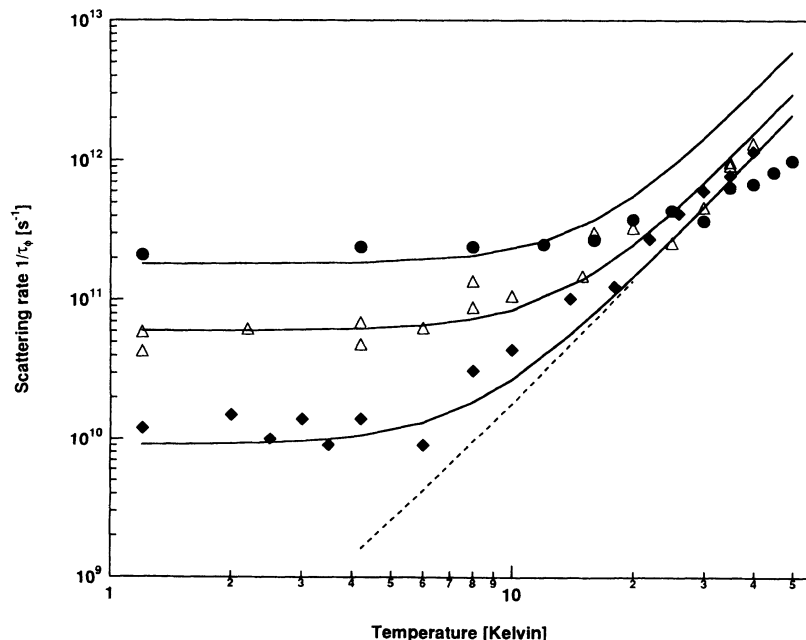

FIG. 6. Dephasing rates shown as a function of the temperature. The symbols denote the dephasing rates as derived from the magnetoresistance measurements. The solid lines and the dashed line are model calculations (not involving fitting) with and without the magnetic scattering, respectively. (♦) 100-nm IBS α-$FeSi_2$, (△) 70-nm SSR α-$FeSi_2$, and (●) 35-nm SSR α-$FeSi_2$.

(open symbols) shown in Fig. 5 saturates at temperatures below 6 K, and decreases with increasing temperature in agreement with an increasing strength of the dephasing scattering due to increased electron-phonon or electron-electron scattering. Different temperature regimes are observed for the α-$FeSi_2$ layers produced by IBS and SSR. However, for temperatures above 20 K the coherence length exhibits the same temperature dependence for the thicker layers, while the thinnest layer (35 nm) shows a weaker temperature dependence. The coherence length for the 100-nm IBS samples shows a $T^{-1.5}$ power-law behavior above 6 K and is in saturation below that temperature. For the solid-state reacted 70-nm layers a saturation in L_ϕ is found below 6 K, a $T^{-0.6}$ power-law behavior between 6 and 20 K, and a $T^{-1.5}$ behavior above 20 K. The 35-nm SSR sample shows a $T^{-0.5}$ power-law behavior above 10 K, and shows a different temperature dependence of the coherence length than observed for the thicker $FeSi_2$ layers. The derived spin-orbit mean-free path (solid symbols) is found to be independent of the temperature for all samples investigated. In Fig. 6 the dephasing-relaxation rates derived from the magnetoresistance measurements are shown. Compared to the other samples, the thinnest solid-state reacted $FeSi_2$ shows a significantly different temperature dependence of the dephasing-scattering rate.

V. DISCUSSION

A thickness dependence of the residual resistivity has been found. Furthermore, the residual resistivity varies inversely with the layer thickness. Such a thickness dependence[43] is in general interpreted as being due to surface[44] or grain boundary[45,46] scattering. Recently also manifestations of quantum-size effects in thin metallic films have been proposed to yield a similar thickness dependence of the resistivity.[47] Both quantum-size and classical-size effects are not expected to contribute significantly to the resistivity in our work because of the relative thick films studied. It is suggested that the thickness dependence observed in this work might be due to grain boundary scattering.

Recent experiments have shown that for some materials the electrical resistivity passes through a minimum when the temperature is lowered, and then increases again when the temperature is further decreased. This nonconventional temperature dependence of the electrical resistivity has been observed in silicide systems such as $MoSi_2$ (Ref. 48) and FeSi,[49] and has, for example, been explained by the Kondo effect.[50] By applying a magnetic field the Kondo effect should disappear, giving rise to a negative magnetoresistance.[51] The observed minimum in the electrical resistivity and the subsequent increase with decreasing temperature is not believed to be due to magnetic impurity scattering because of the small effect an applied magnetic field has on the resistivity. The applied magnetic field tends to enhance the scattering, giving rise to a positive magnetoresistance, and not reducing it as would be expected if the minimum had been due to the Kondo effect. The magnetoresistance of the α-$FeSi_2$ layers shown in Fig. 3 is positive, excluding the influence of the Kondo effect, and the theory of weak localization and spin-orbit interaction has successfully been applied to describe the observed magnetoresistance. The Coulomb interaction resulting in spin splitting of the conduction-electron energies has been proposed to account for the decrease in resistivity with increasing temperatures.[37] From Eq. (7) a $\sqrt{T}$ dependence of the electrical resistivity is predicted. This behavior is clearly observed in the low-temperature dependence of the electrical resistivity as shown in Fig. 2. Furthermore, an approximately T^3 law is found for the dephasing-scattering rate by fitting of Eqs. (4), (5), and (7) to the low-temperature behavior of the electrical resistivity. This implies that the interband *s-d* electron scattering is important in this material, and is consistent with the overall temperature dependence of the electrical resistivity. The SOI scattering rate $1/\tau_{SO}$, or mean-free path L_{SO}, extracted from the data shown in Fig. 2, is found to be in good agreement with those obtained from the magnetoresistance measurements. A $1/\tau_{SO}$ (L_{SO}) value between 1.4×10^{12} s^{-1} (15 nm) and 1.8×10^{12} s^{-1} (15 nm) is found for the 100-nm IBS and 70-nm SSR layers, consistent with the spin-orbit scattering rate found from the magnetoresistance measurements of 1.7×10^{12} s^{-1} (16 nm) and 2×10^{12} s^{-1} (16 nm). The average spin-orbit diffusion length is found to be about 16 ± 2 nm. An estimate of the importance and physical validity of the spin-orbit scattering rate in metals can be obtained by considering the following relation:[52]

$$\frac{\tau_0}{\tau_{SO}} = \frac{L_0^2}{L_{SO}^2} = (\alpha Z)^4 , \tag{8}$$

where α is the fine-structure constant ($\frac{1}{137}$) and Z is the atomic number of iron ($Z=26$). Thus the theoretically expected spin-orbit interaction is found to be $\approx 1.3\times10^{-3}$, and the experimentally found relations are 3.2×10^{-3} (IBS, $d=100$ nm), 2.7×10^{-3} (SSR, $d=70$ nm), and 1.1×10^{-3} (SSR, $d=35$ nm). The observed spin-orbit interaction in all the samples is in fair agreement with the expected value from Eq. (8). The SOI observed in this paper is also in good agreement with other systems. Ousset *et al.*[16] observe a spin-orbit scattering rate of about 8.5×10^{11} s^{-1} in amorphous V-Si. Using relation (8) and assuming the elastic scattering rate is the same for the two systems one would expect the SOI rate in $FeSi_2$ to be ~ 1.6 times larger than for VSi_2 in fair agreement with the observed spin-orbit scattering rate.

As mentioned in Sec. II, the dephasing and spin-orbit interaction scattering rates can be deduced from the nonlinear least-squares fits to the magnetoresistivity measurements. At the lowest temperatures the dephasing rates (coherent lengths) $1/\tau_\phi$ (L_ϕ) are found to saturate and become independent of the temperature (Fig. 6). At temperatures between 4.2 and 20 K the dephasing rate for the SSR layers gives an exponent of 1.2 ± 0.3. The saturation and the weak temperature dependence at the lowest temperatures can be explained by the influence of residual spin scattering arising from magnetic impurities. The saturation of the dephasing rate allows for an estimate of the magnetic scattering rate (mean-free path) $1/\tau_s$ (L_s) which is found to be between 1.2×10^{10} s^{-1} (220

nm) and 4.3×10^{10} s^{-1} (103 nm) for IBS fabricated and SSR layers, respectively. Because of the magnetic-impurity scattering only an upper limit of the inelastic scattering rates, due to, for example, electron-phonon scattering, can be obtained at the lowest temperatures. The inelastic scattering rates, excluding the residual spin scattering, are much lower than the dephasing rates. Thus the coherence length L_ϕ is found to be fairly large at low temperatures. Between 1 and 20 K L_ϕ is much larger than both the elastic mean-free path L_0 and the spin-orbit diffusion length L_{SO} which is a criterion for weak localization. The temperature dependence of the dephasing scattering rate, described by the power law $A_\phi T^{p_\phi}$, is found to be dominated by electron-phonon *s-d* interband scattering at higher temperatures (IBS: $T>6$ K; SSR: $T>20$ K) giving rise to an exponent $p_\phi\approx3$. This is expected for materials consisting of a transition-metal component, and is furthermore, in agreement with the analysis of the temperature dependence of the electrical resistivity at zero magnetic field. Table I summarizes the dephasing-scattering rate obtained by magnetoresistance, low-temperature dependence of the electrical resistivity, and from the Bloch-Grüneisen analysis (see below). This clearly shows that the temperature dependence of the dephasing-scattering rate is found to agree well between the different experimental techniques used. The differences in the prefactors are reflected in the standard deviations of the exponents. A significant difference in the temperature dependence of the coherence scattering rate obtained by the magnetoresistance and the electrical resistivity is, however, observed for the thinnest SSR $FeSi_2$. It is suggested that this difference might be due to an enhanced importance of the magnetic impurities present in the sample as compared to the relative thicker samples. A general expression for the electron-electron scattering rate[53] and the electron-phonon[54] contribution in disordered metals can be written as

$$\frac{1}{\tau_\phi}=\frac{1}{\tau_{ee}}+\frac{1}{\tau_{ep}}=\left[\frac{\pi}{8}\frac{k_B^2}{\hbar E_F}T^2+\frac{\sqrt{3}}{1}\frac{1}{(k_FL_0)^{3/2}}\frac{k_B^{3/2}}{\hbar\sqrt{E_F}}T^{3/2}\right]_{e\text{-}e}+[A_{e\text{-ph}}T^3]_{e\text{-ph}} . \tag{9}$$

The Fermi energy E_F and k_FL_0 have been obtained from the Hall measurements (see Table II). The electron-phonon interaction strength $A_{e\text{-ph}}$, as derived by Schmid,[54] assuming only *s*-wave scattering, is given by

$$A_{e\text{-ph}}=\frac{2\pi}{3}N(E_F)g^2\frac{k_B}{\hbar\Theta^2} , \tag{10}$$

where g is the electron-phonon coupling strength $g=(\hbar k_F)^2/3mv\sqrt{d}$ (v being the sound velocity, and d the material density). By calculating the sound velocity in $FeSi_2$ using the Bohm-Staver relation,[55] and the density of states $N(E_F)$ obtained from the Hall measurements, and assuming that the Debye temperature Θ is 500 K, the $A_{e\text{-ph}}$ is found to be about 2×10^4 $s^{-1}K^{-3}$ [or $\approx1\times10^6N(E_F)g^2$ $s^{-1}K^{-3}$], which is at least two orders of magnitude less than observed in Fig. 6. It is believed that the assumption of scattering only from *s* states is the reason for the large difference between the theoretical and the experimentally observed values. This assumption leads to a too low electron-phonon coupling strength. Comparison with the experimental data in Fig. 6 indicates that $N(E_F)g^2$ should be at least equal to 1. However, using the Bloch-Grüneisen model for the electron-phonon scattering, due to interband scattering [see Eq. (1)], a semiquantitative estimate of $A_{e\text{-ph}}$ can be found,

$$A_{e\text{-ph}}\approx7.21\frac{pe^2}{m^*}\frac{\rho'}{\Theta^2} , \tag{11}$$

where p is the hole carrier concentration, m^* is the effective hole mass, ρ' the electron-phonon resistivity prefactor, and Θ the effective Debye temperature. The carrier concentration has been obtained from the Hall measurements (see Table II), ρ' and Θ have been obtained from a nonlinear fit to the temperature dependence of the resistivity shown in Fig. 1. Thus all the parameters in Eqs. (9) and (11) are known quantities, and the order of magnitude of the dephasing scattering rate can be assessed. The result of such a calculation is shown in Fig. 6 and summarized in Table III. The obtained dephasing scattering rate, illustrated by the dashed line in Fig. 6, is obviously too low at the lowest temperatures, compared with the experimental results. One reason for this is due to scattering from magnetic impurities that is independent of the temperature, and would give an additional

TABLE III. Model calculation of the dephasing scattering rate $1/\tau_\phi$, using parameters estimated from the Hall effect measurements and from the Bloch-Grüneisen theory.

Sample	Eq. (9)
IBS	
$d=100$ nm	$\frac{1}{\tau_\phi}=[2.0\times10^6T^2+38.0\times10^6T^{3/2}]_{e\text{-}e}+[16.6\times10^6T^3]_{e\text{-ph}}\,s^{-1}$
SSR	
$d=70$ nm	$\frac{1}{\tau_\phi}=[2.2\times10^6T^2+50.6\times10^6T^{3/2}]_{e\text{-}e}+[23.0\times10^6T^3]_{e\text{-ph}}\,s^{-1}$
SSR	
$d=35$ nm	$\frac{1}{\tau_\phi}=[1.9\times10^6T^2+131.2\times10^6T^{3/2}]_{e\text{-}e}+[45.6\times10^6T^3]_{e\text{-ph}}\,s^{-1}$

constant contribution to the scattering rate in Eq. (9). However, if the derived magnetic-scattering rate is added to the dephasing rate a qualitatively good agreement with the experimental results is obtained as shown in Fig. 6 (solid lines). Although the magnetic scattering makes it difficult to probe the effect of electron-electron interaction on the magnetoresistance, this effect can be observed when combined with the analysis of the low-temperature dependence of the electrical resistivity.

VI. CONCLUSION

The behavior of the low-temperature electrical resistivity and magnetoresistance of the α-$FeSi_2$ has been thoroughly analyzed, and it has been shown that quantum corrections to the electrical resistivity have to be considered in order to explain the experimental results. The polycrystalline materials are found to be highly disordered with a disorder parameter $(k_F L_0)^{-1}$ between 0.14 and 0.33 for the thickest and thinnest layers, respectively. A thickness dependence of the residual resistivity has been found which is suggested to be due to grain boundary scattering.

Both weak-localization, including a strong spin-orbit coupling, and electron-electron interactions originating from the particle-hole channel are used to describe the magnetoresistance and the low-temperature dependence of the electrical resistivity. The length scales obtained for the different scattering mechanisms are consistent with the observation of weak-localization effects. The elastic mean-free path L_0 is found to be between 0.38 nm for the 35-nm layer and 0.90 nm for the 100-nm layer. The coherence length L_ϕ is found to be at least 100 nm, and the spin-orbit interaction length L_{SO} to be about 16 nm. Therefore the condition for weak localization $L_\phi / L_0 > L_{SO}/L_0 \gg 1$ is clearly fulfilled. Furthermore, no anomalous high spin-orbit coupling strength, as reported in other publications,[11] is found in this work. The spin-orbit strength as compared to the elastic scattering is in very good agreement with the expected value, and is found to be temperature independent, and independent of sample fabrication technique. Comparison of the dephasing rate obtained from the magnetoresistance measurements with the ones obtained from fitting to the low-temperature behavior of the electrical resistivity shows that the dephasing is mainly due to electron-phonon *s-d* interband scattering. The dephasing exponent is consistent with the result of the Bloch-Grüneisen analysis, where the best agreement between the measured electrical resistivity and the model is found for an exponent of 3.

ACKNOWLEDGMENTS

The authors are pleased to acknowledge Rita Verbeeck and Joris Van Laer for technical assistance. K.K.L. acknowledges the financial support from the European Union's Human Capital and Mobility program. A.L. is indebted to the Belgian Institute for Scientific Research in Industry and Agriculture (IWONL). K.M. is a Research Associate of the Belgian National Fund for Scientific Research.

[1] L. J. Chen and K. N. Tu, Mater. Sci. Rep. **6**, 53 (1991).
[2] H. von Känel, Mater. Sci. Rep. **8**, 193 (1992).
[3] K. Maex, Mater. Sci. Rep. **R11**, 53 (1993).
[4] J. C. Hensel, in *Thin Films—Interfaces and Phenomena*, edited by R. J. Nemanich, P. S. Ho, and S. S. Lau, MRS Symposia Proceedings No. 54 (Materials Research Society, Pittsburgh, 1986), p. 499.
[5] F. Nava, K. N. Tu, O. Thomas, J. P. Senateur, R. Madar, A. Borghesi, G. Guizzetti, U. Gottlieb, O. Laborde, and O. Bisi, Mater. Sci. Rep. **9**, 141 (1993).
[6] P. L. Rossiter, *The Electrical Resistivity of Metals and Alloys* (Cambridge University Press, Cambridge, England, 1987).
[7] E. Abrahams, P. W. Anderson, D. C. Licciardello, and T. V. Ramakrishnan, Phys. Rev. Lett. **42**, 673 (1979).
[8] H. Fukuyama and K. Hoshino, J. Phys. Soc. Jpn. **50**, 2131 (1981).
[9] P. A. Lee and T. V. Ramakrishnan, Phys. Rev. B **26**, 4009 (1982).
[10] A. I. Larkin, Pis'ma Zh. Eksp. Teor. Fiz. **31**, 239 (1980) [JETP Lett. **31**, 219 (1980)].
[11] K. Radermacher, D. Monroe, A. E. White, K. T. Short, and R. Jebasinski, Phys. Rev. B **48**, 8002 (1993).
[12] M. A. Howson and B. L. Gallagher, Phys. Rep. **170**, 265 (1988).
[13] N. Karpe, K. Kyllesbech Larsen, and J. Bøttiger, Phys. Rev. B **46**, 2686 (1992).
[14] T. Klein, C. Berger, D. Mayou, and F. Cyrot-Lackmann, Phys. Rev. Lett. **66**, 2907 (1991).
[15] A. Sahnoune, J. O. Ström-Olsen, and A. Zaluska, Phys. Rev. B **46**, 10 629 (1992).
[16] J. C. Ousset, H. Rakoto, J. M. Broto, V. Dupuis, and S. Askenazy, Phys. Rev. B **36**, 5432 (1987).
[17] S. Mantl, Mater. Sci. Rep. **8**, 1 (1992).
[18] K. Kyllesbech Larsen, A. Lauwers, K. Maex, and M. Van Rossum, in *Silicides, Germanides, and their Interfaces*, edited by R. W. Fathauer, L. Schowalter, S. Mantl, and K. N. Tu, MRS Symposia Proceedings No. 320 (Materials Research Society, Pittsburgh, in press).
[19] F. J. Blatt, *Physics of Electronic Conduction in Solids* (McGraw-Hill, New York, 1968).
[20] G. J. Morgan, M. A. Howson, and K. Saub, J. Phys. F **13**, 2127 (1983).
[21] G. F. Wier and G. J. Morgan, Philos. Mag. **47**, 177 (1983).
[22] D. Rainer and G. Bergmann, Phys. Rev. B **32**, 3522 (1985).
[23] J.-B. Bieri, A. Fert, and G. Creuzet, Solid State Commun. **49**, 849 (1984).
[24] K. Maki, Prog. Theor. Phys. **39**, 897 (1968); **40**, 193 (1968).
[25] R. S. Thompson, Phys. Rev. B **1**, 327 (1970).
[26] A. Kawabata, Solid State Commun. **34**, 431 (1980).
[27] J. C. Ousset, S. Askenazy, H. Rakoto, and J. M. Broto, J. Phys. (Paris) **46**, 2145 (1985).
[28] D. J. Thouless, Phys. Rev. Lett. **39**, 1167 (1977).
[29] P. A. Lee and T. V. Ramakrishnan, Rev. Mod. Phys. **57**, 287 (1985).

[30]L. P. Gor'kov, A. I. Larkin, and D. E. Khmelnitzkii, Pis'ma Zh. Eksp. Teor. Fiz. **30**, 248 (1979) [JETP Lett. **30**, 248 (1979)].
[31]Y. Isawa and H. Fukuyama, J. Phys. Soc. Jpn. **53**, 1415 (1984).
[32]H. Fukuyama, J. Phys. Soc. Jpn. **51**, 1105 (1982).
[33]A. Sahnoune, J. O. Ström-Olsen, and H. E. Fischer, Phys. Rev. B **46**, 10 035 (1992).
[34]P. Vandenabeele and K. Maex, J. Vac. Sci. Technol. A **9**, 2784 (1991).
[35]S. L. Hsia, T. Y. Tan, P. Smith, and G. E. McGuire, J. Appl. Phys. **70**, 7579 (1991).
[36]K. Kyllesbech Larsen *et al.* (unpublished).
[37]T. B. Massalski, *Binary Alloy Phase Diagrams* (American Society for Metals, Metal Park, OH, 1986).
[38]K. Radermacher, S. Mantl, D. Gerthsen, Ch. Dieker, and H. Lüth, Nucl. Instrum. Methods Phys. Res. Sect. B **80/81**, 831 (1993).
[39]M. Gurvitch, Phys. Rev. B **24**, 7404 (1981).
[40]P. B. Allen, W. E. Pickett, K. M. Ho, and M. L. Cohen, Phys. Rev. Lett. **40**, 1532 (1978).
[41]N. E. Christensen (private communication).
[42]J. Friedel, in *The Physics of Metals,* edited by J. M. Ziman (Cambridge University Press, New York, 1969).
[43]J. R. Samples, Thin Solid Films **106**, 321 (1983).
[44]K. Fuchs, Proc. Cambridge Soc. Philos. **34**, 100 (1938).
[45]A. F. Mayadas, M. Shatzkes, and J. F. Janak, Appl. Phys. Lett. **14**, 345 (1969).
[46]G. Reiss, J. Vancea, and H. Hoffmann, Phys. Rev. Lett. **56**, 2100 (1986).
[47]N. Trivedi and N. W. Ashcroft, Phys. Rev. B **38**, 12 298 (1988).
[48]J. W. C. de Vries and A. H. van Ommen, J. Appl. Phys. **64**, 749 (1988).
[49]M. Onda, H. Sirringhaus, P. Steiner, and H. von Känel, in *Evolution of Surface and Thin Film Microstructure,* edited by H. A. Atwater, E. Chason, M. Grabow, and M. Lagally, MRS Symposia Proceedings No. 280 (Materials Research Society, 1993), p. 473.
[50]J. Kondo, in *Solid State Physics: Advances in Research and Applications,* edited by F. Seitz (Academic, New York, 1969), Vol. 23, p. 184.
[51]A. A. Abrikosov, *Fundamentals of the Theory of Metals* (North-Holland, Amsterdam, 1988).
[52]A. A. Abrikosov and L. P. Gorkov, Zh. Eksp. Teor. Fiz. **24**, 1088 (1962) [Sov. Phys. JETP **15**, 752 (1962)].
[53]A. Schmid, Z. Phys. **271**, 251 (1974).
[54]A. Schmid, Z. Phys. **259**, 421 (1973).
[55]D. Bohm and T. Staver, Phys. Rev. **84**, 836 (1950).